Chapter 21
Detection of Infrasound Signals and Sources Using a Dense Seismic Network

Catherine de Groot-Hedlin and Michael Hedlin

Abstract This new era of massive datasets gives us the opportunity to examine Earth structure and geophysical phenomena in more detail than previously possible. Large datasets hold much promise for transformative research but require new analytical methods that are both efficient and capable of extracting useful information from faint signals immersed in noise. With these needs in mind, we developed the AELUMA (Automated Event Location Using a Mesh of Arrays) method that recasts any dense network of sensors as a distributed mesh of small triangular arrays (triads). Each array provides a local estimate of signal properties. Information from arrays distributed across the footprint of the network is combined to estimate the source origin time and location. The process is repeated without oversight to catalog events that have occurred over a period of time. We have analyzed ground-coupled airwaves recorded on vertical component broadband seismometers of the USArray Transportable Array (TA). We estimate the accuracy of the AELUMA algorithm using ground truth events at the Utah Test and Training Range (UTTR). In a study of 23 surface explosions, the mean AELUMA source location estimate is 8.6 km northwest of the ground truth location. The origin time estimates were late for most events. The mean time misfit is 19 s with a standard deviation of 39 s. We attribute the positive bias in origin time estimates to signal dispersion, as the AELUMA method estimates the time of the signal's peak amplitude, not its onset. A comparison of AELUMA and a reverse time migration method indicates that AELUMA is more sensitive to faint signals from weak events and the event locations are more accurate in space and time. A catalog of acoustic activity from across the continental United States in the band from 0.7 to 4.0 Hz includes 7935 events that were detected by 10 or more triads. Most events were clustered into hotspots and are likely anthropogenic.

C. de Groot-Hedlin (✉) · M. Hedlin (✉)
Laboratory for Atmospheric Acoustics, Institute of Geophysics and Planetary Physics, Scripps Institution of Oceanography, University of California, San Diego, La Jolla, CA 92093-0225, USA
e-mail: chedlin@ucsd.edu

M. Hedlin
e-mail: hedlin@ucsd.edu

A. Le Pichon et al. (eds.), *Infrasound Monitoring for Atmospheric Studies*,
https://doi.org/10.1007/978-3-319-75140-5_21

21.1 Introduction

A new technique to detect geophysical signals within a dense sensor network, called Automated Event Location Using a Mesh of Arrays (AELUMA), was described by de Groot-Hedlin and Hedlin (2015). The AELUMA method relies on partitioning a network of sensors into large ensembles of three-element arrays, enabling the identification of weak sources that generate detectable signals over a subset of the network sensors. The method is not strongly dependent upon the characteristics of the propagation medium and can be applied to identifying a wide range of signal types. For instance, variations of this method have been applied to the detection of gravity waves generated by a severe storm system (de Groot-Hedlin et al. 2013), to seismic source detection, as well as the detection of infrasound sources at USArray pressure sensors (de Groot-Hedlin and Hedlin 2015). In this chapter, it is applied to detecting and cataloging infrasound sources using seismic sensor data. This allows for the identification of repeating sources that can be used to study the temporal variability of the infrasonic wave field (Gibbons et al. 2019).

Infrasonic waves can propagate to ranges up to thousands of kilometers through ducts formed by the stratification of temperatures and winds in Earth's atmosphere (Drob et al. 2003; Evers and Haak 2010, and references therein). Multiple infrasound signals separated by several minutes are sometimes observed at a single source–receiver pair (Hedlin et al. 2010; Fee et al. 2013), each arrival having traveled along a distinct propagation path. Most infrasound signals travel through tropospheric ducts, which result from nocturnal temperature inversions (Fee and Garcés 2007) or the tropospheric wind jet (Fee et al. 2013), or stratospheric ducts, caused by seasonally varying stratospheric winds (Drob et al. 2003). The existence of these temporally and spatially varying ducts often determines whether or not infrasonic signals are recorded at the Earth's surface (e.g., Le Pichon et al. 2009; de Groot-Hedlin et al. 2010, and references therein). Observations of thermospherically ducted energy are comparatively infrequent because infrasound undergoes significant intrinsic attenuation within the rarefied upper atmosphere (Sutherland and Bass 2004). Since acoustic absorption increases with frequency, thermospherically ducted signals are associated only with sources that generate significant low-frequency infrasonic energy (e.g., Garcés et al. 2004; de Groot-Hedlin and Hedlin 2014a, b; Pilger et al. 2015).

Infrasonic waves have been to study energetic sources like meteors and bolides (Revelle et al. 2004; Ishihara et al. 2004; Pilger et al. 2019; Silber and Brown 2019), volcanoes (Delclos et al. 1990; Matoza et al. 2009; Fee and Matoza 2013; Matoza et al. 2019; Marchetti et al. 2019), auroral arcs (Pasko 2012), and tsunami-genic earthquakes (Walker et al. 2013; Le Pichon et al. 2005c). Anthropogenic sources can also be powerful sources of infrasound signals (Campus and Christie 2010), including mining blasts (Hagerty et al. 2002; Gibbons et al. 2019), chemical explosions (Öttemoller and Evers 2008; Ceranna et al. 2009; Vergoz et al. 2019),

and supersonic aircraft including the Concorde (Le Pichon et al. 2002) and the space shuttle Atlantis (de Groot-Hedlin et al. 2008). Infrasound has also proven useful in investigating the nature of the propagation medium—the Earth's atmosphere. A basic formalism for applying passive acoustic remote sensing techniques to infrasound data was presented by Drob et al. (2010). Infrasound recordings have been used to study atmospheric dynamics up to the lower thermosphere (Donn and Rind 1971; Garcés et al. 2004; Le Pichon et al. 2005a, b; Assink et al. 2013, 2019; Chunchuzov et al. 2015; Smets et al. 2016), and to investigate the effects of gravity waves on infrasound signal coda (e.g., Millet et al. 2007; Kulichkov et al. 2010; Green et al. 2011; Hedlin and Drob 2014; Lalande and Waxler 2016; Chunchuzov and Kulichkov 2019).

Infrasound is one of the four primary technologies in monitoring the Comprehensive Nuclear-Test-Ban Treaty (CTBT) (Campus and Christie 2010). Infrasonic waves are continuously recorded at a global network of infrasound sensors deployed as one component of the International Monitoring Systems (IMS) (Christie and Campus 2010), designed to monitor compliance with the CTBT. The network is designed to have a uniform distribution of stations over the globe, at an average interstation spacing of approximately 2000 km. However, due to the sparse station sampling, many infrasound signals detected at this network have an unknown origin (Campus and Christie 2010; Marty 2019). Matoza et al. (2017) and Arrowsmith et al. (2015) developed automated methods of detecting and locating infrasound signals from explosive volcanic events using IMS infrasound network data.

In recent years, infrasound networks with much denser spatial sampling have been deployed, allowing for more detailed studies of infrasound sources and of infrasound propagation characteristics. Data from the Large Aperture Infrasound Array (LAIA) in the Netherlands, which comprises 30 receivers and has an aperture of 100 km, have been used in interferometric studies to estimate the temporal variability of tropospheric wind and sound speeds (Fricke et al. 2014). The USArray Transportable Array (TA) is a semi-permanent network that comprises 400 infrasonic stations installed in a nearly regular east–west/north–south Cartesian grid distributed over a 2,000,000 km^2 area between the Mexican and Canadian borders, with an average interstation spacing of 70 km. The TA gradually moved eastward at an average pace of ~500 km/year through station redeployments. This network has allowed for the detection and identification of much smaller sources than would be observed at much sparser station spacing (Edwards et al. 2014; de Groot-Hedlin and Hedlin 2015).

The infrasonic network is one component of the TA network, which originated as a seismic observatory (Busby et al. 2006) intended for studies of seismic sources and the Earth's interior. The seismic TA network was initially deployed along the west coast in 2004. It was not until mid-2010, when the TA was located in the central United States, that infrasound sensors were installed along with the broadband seismometers at each site, transforming it into a large seismo-acoustic network (Vernon et al. 2012). However, it is well understood that infrasound signals couple to seismic waves at the Earth's surface and are often recorded on seismometers (Arrowsmith et al. 2010). These ground-coupled airwaves arise when

acoustic waves couple to Rayleigh waves at the Earth's surface (Crampin 1966; Edwards et al. 2007). Infrasonic waves recorded at seismic networks have been used to localize infrasound sources (Cochran and Shearer 2006; Fee et al. 2016). Seismic data from the TA have been used for infrasound studies in the western US (de Groot-Hedlin et al. 2008; Hedlin et al. 2010; Walker et al. 2010). Walker et al. (2011) constructed an infrasound event catalog by applying a Reverse Time Migration (RTM) to TA seismic sensor data.

New analytic methods of detecting and locating infrasonic signals hold the promise of providing extensive catalogs of sources that can be used either for basic infrasound research or to understand the background noise that may hamper efforts in monitoring nuclear test ban treaties. Section 21.2 reviews previously published methods of locating infrasound sources using array data. Section 21.3 introduces the TA seismic data used to develop a catalog of infrasound events for the continental United States and describes the ground truth data used to verify the accuracy of the AELUMA algorithm. The AELUMA method and its application to seismic data are described in Sect. 21.4. Section 21.5 presents the view of acoustic sources and noise in the continental US that results from applying AELUMA to 9 years of TA seismic data. Section 21.6 compares the sensitivity of the AELUMA method to previously published results. Conclusions are stated in Sect. 21.7.

21.2 Infrasound Source Location Methods

Infrasound source location estimates are adversely affected by spatial and temporal variations in sound and wind speeds, especially for sparse networks. Evers and Haak (2005) observed that infrasonic waves generated by eruptions of Mt. Etna at infrasonic arrays located in the Netherland and Germany, at ranges over 1000 km, were deflected by stratospheric winds. The resulting deflections in the measured azimuths at these arrays led to an error of nearly 100 km in the apparent source location. Arrowsmith et al. (2015) and Matoza et al. (2017) developed algorithms to detect and catalog event using only data from global the IMS infrasound stations; in both studies, some source locations were mis-estimated by over 100 km. Another drawback of using only the IMS network is that only very energetic sources are detectable at two or more stations. The global IMS infrasound network is designed to reliably detect atmospheric explosions with yields of at least 1 kT (Le Pichon et al. 2009), which may be an unreachable goal with the current sparse IMS infrasound network (Arrowsmith et al. 2015). Additional data from regional networks are often needed to improve source identification (Campus and Christie 2010) and location (Matoza et al. 2017).

Arrowsmith et al. (2008) presented an automated technique for the detection and location of infrasound events using data from two regional infrasound networks: one in Utah that comprised three arrays separated by approximately 80 km, and one in Washington state that included three arrays separated by 200–300 km. Processing was performed separately at each network to produce localized source maps

for each region. In another regional infrasound study, Park et al. (2014) developed an automated method to detect infrasound sources in the western US using data from twelve infrasonic arrays, nine located in Utah and three in Nevada. Data from all twelve of these arrays were combined to develop a catalog characterizing regional infrasound sources in the western US from November 2010 through October 2012. They found 1510 events over this time period and identified many of the same acoustic hotspots found in the Walker et al. (2011) study for the 2007–2008 period. Park and Stump (2015) also observed seasonal variations in infrasound source detections that correlated with seasonal variations in stratospheric winds.

Apart from the TA infrasound network and the LAIA in the Netherlands, dense networks are much more common for seismic sensors than for infrasound sensors. This has led to the development of several independent methods of using ground-coupled airwaves to detect and characterize infrasound events. Before the TA was in place, Cochran and Shearer (2006) used seismic data from over 200 stations in the Southern California Seismic Network to identify infrasound events. They used cross-correlation of signal envelopes to locate 76 previously undetected infrasound sources in 2003. Fee et al. (2016) applied several methods to detect volcanic explosions recorded on volcano-seismic networks in Alaska. For sources that were far from the network, they assumed that infrasonic waves crossing the network were roughly planar and applied an f-k analysis to estimate the phase velocity and the azimuth to source. For source located within the network, they used differential travel times between station pairs found by cross-correlating waveform envelopes to invert for source parameters.

Walker et al. (2011) used an RTM method to detect infrasound sources recorded at TA seismic sensors and construct maps of "acoustic hotspots" in the western US. RTM is a standard geophysical method that relies on the assumption that energy originates at a single point in a medium with known velocities; records are aligned for travel times corresponding to the known velocities and a grid of candidate source locations and stacked. The source location corresponds to the stack with the greatest constructive interference. An advantage of the RTM method is that it is broadly applicable to data from both dense arrays and sparser networks. A drawback is that the stacking velocities must be accurately known. Walker et al. (2011) used a constant stacking velocity and very sparse time sampling rate, thus smoothing the envelopes and limiting the size of the infrasound sources that could be detected. Although the accuracy could be improved with more accurate information about the range- and azimuth-dependent celerity of the medium, this is complicated by the temporally varying nature of wind and sound speeds that govern infrasound velocities.

21.3 Dataset

21.3.1 Ground Truth Sources

Rocket motor fuel blasts conducted at the Utah Test and Training Range (UTTR) offer a natural laboratory for infrasound propagation research. In this study, these sources are used to assess the precision, accuracy, and sensitivity of the AELUMA method and make possible a direct comparison with the RTM method. The UTTR facility, located approximately 130 km west of Salt Lake City, is used for military training and testing, as well as the disposal of explosive ordnance. Each year a number of rocket motors from Trident long-range missiles are destroyed as required by an agreement between the United States and Russia. Because of its location west of Salt Lake City, these detonations occur only during the summer so that stratospheric winds from the east can be relied on to carry much of the acoustic energy away from the city. These sources are very useful for assessing detection/location algorithms given that the sources are large, impulsive, repeating, and have accurately known source locations and detonation times.

The detonations that occurred at UTTR in 2007 and 2008 are listed in Table 21.1. All explosions occurred on a semi-circular pad at 41.13152°N, 112.89577°W, and origin times are reported to the nearest second (personal communication, Relu Burlacu, University of Utah). Explosive yields are reported in pounds and converted to the nearest kg. Table 21.1 summarizes ground truth information on 21 explosions at UTTR in the 2 years (12 in 2007, the remainder in 2008). All explosions except one had a reported explosive yield of approximately 17,500 kg with one considerably smaller (7955 kg) detonation.

21.3.2 Seismic Data

In this study, vertical component broadband seismic data recorded at the USArray Transportable Array from January 1, 2006 through the end of 2014 (Fig. 21.1) are used to detect and catalog infrasound sources. First, data recorded in 2007 and 2008 are used to assess the accuracy and sensitivity of AELUMA, and to directly compare it with the RTM method of Walker et al. (2011). During these years, the bulk of the TA was located downwind of the UTTR facility (Fig. 21.1) and did not yet include infrasonic microphones. At the beginning of the study period, the TA comprised only 311 stations but a full complement of 470 stations was available by the end of 2008. Various networks were incorporated into the TA during this time period (see anf.ucsd.edu).

Table 21.1 UTTR event origin dates/times and explosive yields. The AELUMA results were based on detections in the 0.7–4 Hz band. T_{miss} is AELUMA origin time minus GT origin time (i.e., positive values means AELUMA origin time is late). D_{miss} is the distance between the AELUMA location estimate and the known UTTR source location

Year/day	GT-OT	Expl. Yield	AELUMA-OT	T_{miss}	D_{miss}	# triads
	(UTC)	(kg)	(UTC)	(s)	(km)	
2007135	19:30:48	17634	19:31:30	42	16.79	60
2007155	19:52:21	17597	19:52:40	19	13.31	57
2007162	19:49:24	17688	19:49:20	−4	15.80	93
2007177	19:43:20	17688	19:43:50	30	21.60	91
2007190	21:38:37	17634	21:37:50	−47	9.83	96
2007197	17:33:31	17634	17:35:10	99	34.04	100
2007213	20:01:24	17634	20:01:50	26	22.96	109
2007218	20:33:03	17634	20:33:40	37	19.67	100
2007225	19:38:21	17634	19:39:00	39	21.22	94
2007239	20:43:12	17634	20:44:15	58	8.79	104
2007253	17:33:02	17634	17:33:10	8	3.53	34
2007260	20:21:38	17634	20:22:30	12	6.54	38
2008168	20:32:27	17597	20:32:20	−7	9.42	45
2008175	20:12:14	17143	20:13:00	46	9.84	68
2008189	20:16:23	17688	20:16:30	7	10.51	57
2008197	20:05:46	17688	20:05:50	4	5.74	40
2008203	17:56:39	17688	17:57:00	21	9.43	37
2008212	20:20:24	17688	20:21:50	86	2.08	31
2008217	20:06:29	17688	20:05:50	−39	4.73	27
2008224	19:52:03	7955	19:51:00	−63	14.94	19
2008232	20:49:32	17688	20:50:00	28	12.88	19
2008254	17:02:11	Not known				
2008261	16:54:50	Not known				

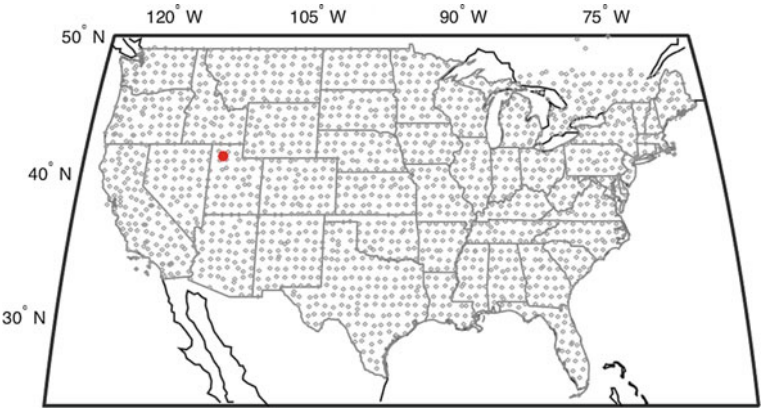

Fig. 21.1 A total of 1,986 broadband seismic stations operated in the TA from 2004 through 2015. At any given time, an average of about 400 stations was running. Explosions at the UTTR facility in Utah were used to assess location accuracy (red dot)

21.4 The AELUMA Source Location Method

An automated method to detect and locate infrasound sources using signals recorded at a dense network of seismic stations is described in this section. This approach builds on the AELUMA algorithm, first described in de Groot-Hedlin and Hedlin (2015), which was applied to data collected by infrasound microphones deployed at USArray Transportable Array (TA) stations in the eastern United States. In this method, a large network of sensors is recast as a mesh of small arrays, each comprising three adjacent stations. Data from each three-element array (or "triad") are processed to detect signals that are consistent with plane wave propagation across the triad. When a coherent signal is detected, its phase velocity and direction of propagation are computed. Results from all triads with signal detections are collectively used to automatically and rapidly provide an accurate estimate of the source's origin time and location.

Because seismometers are, by design, more sensitive to seismic energy than to infrasound signals, the basic AELUMA algorithm described in de Groot-Hedlin and Hedlin (2015) has been altered for use in finding infrasound events using seismic data. The steps for the AELUMA method are described for infrasound signals recorded at TA seismometers on day 218 of 2007. The events on this day include a surface explosion at the UTTR facility with an accurately known source time and location. The AELUMA method is applicable to a wide range of signal types and network configurations. The appendix includes a table with a description of the parameters that are used to tune the algorithm to a particular signal type and array configuration, and the values used for this study.

21.4.1 Computation of Waveform Envelopes

For cases where the interstation spacing is small in comparison to the signal wavelength of interest, waveforms from adjacent stations can be cross-correlated to determine whether they are spatially coherent. This was the case in de Groot-Hedlin et al. (2014) where long-period atmospheric gravity waves generated by a tornadic convective storm system were observed crossing the TA. However, because infrasound signals are coherent over distances of several kilometers at most, much less than the typical TA interstation spacing of 70 km, signal envelopes are computed for each waveform and cross-correlations are performed over the demeaned envelopes at adjacent stations. As noted by Fee et al. (2016), acoustic-to-seismic coupling at the Earth's surface leads to incoherent waveforms, even at more closely spaced stations.

The data are examined one day at a time along with 2 h of the following day in order to capture events that occur at the end of the day. Stations are discarded if

there is a gap of more than 1 s in that time interval. A Hilbert transform is applied to band-passed waveform data to compute the initial envelope. A short-term-average over long-term-average (STA/LTA) filter is applied to the initial envelope to enhance small-scale signals, and the result is decimated to 1 point per second. The envelopes are an approximate measure of the signal-to-noise ratio (SNR) of the arrivals. In this study, the time spans chosen for the STA and LTA filters were 10 s and 600 s, respectively, and the frequency range is from 0.7 to 4 Hz.

Band-passed seismic waveforms and associated envelopes are shown in Fig. 21.2 for a 1-h time span for signals from a rocket motor fuel cylinder blast at the Utah Test and Training Range (UTTR). This surface explosion generated infrasound signals that were recorded over a wide area to the west of the blast, as well as seismic signals detected over a smaller radius near the event. The east–west transect in Fig. 21.2 shows that the amplitudes of the earlier-arriving seismic signals are much higher than for infrasound signals near the source, but they decrease much more rapidly with distance. At least two more seismic signals can be seen in this 1 h time span, a larger one at about 21:10 UT and a smaller one at 21:25 UT; these arrivals are characterized by their much higher velocity than for the infrasound signals.

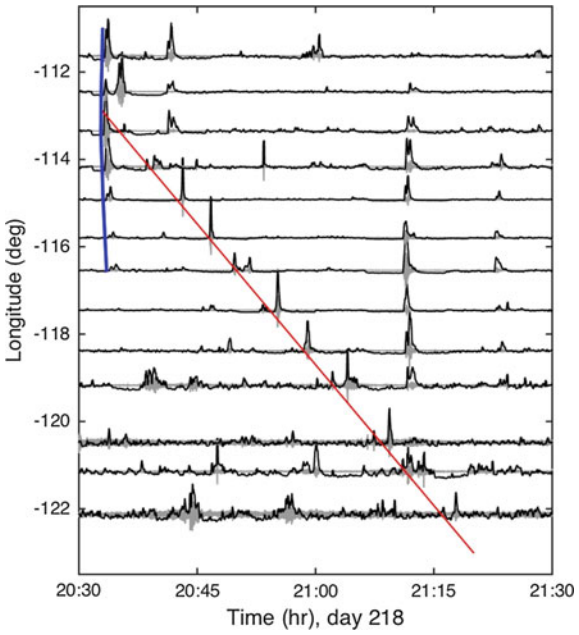

Fig. 21.2 An east–west transect through the TA within a latitude range of 41–41.7°N shows signals from a 17,634 kg surface explosion that occurred at time 20:33:03 UT on day 218, 2007, at UTTR [41.131°N, −112.8965°E.]. The band-passed waveforms are shown in gray, and their envelopes are shown in black. The data and envelopes are scaled such that the maxima are equal for all waveforms. The blue curve shows seismic arrivals from the UTTR blast; the red line indicates infrasound signals. Seismic signals from unrelated events arrive at about 21:10 and 21:25 UT

21.4.2 Network Discretization and Array Analysis at Each Triad

The TA network has a slightly different configuration from day to day due to data availability at individual stations, or as sites are either deployed or removed from the network. For any given day, the network of available stations is discretized into a nonoverlapping mesh of small triangular arrays, each composed of three adjacent stations. Although there are many ways of triangulating any given set of points, the array analysis is ideally performed on triads with equal side lengths. For that reason, a Delaunay triangulation (Lee and Schachter 1980) is used as it avoids triangulations that include triangles with very small interior angles. However, given the configuration of the TA, some highly obtuse triangles remain after the Delaunay triangulation step, so all triads with interior angles greater than 130° or less than 15° are eliminated from further analysis. Triads with arm lengths over 150 km, about twice the average station separation, are also eliminated.

A two-step array analysis is performed at each triad; first signals consistent with the passage of a plane wave across the array are sought and then, once found, the azimuth and phase velocity for each of these signals is computed. To detect coherent signals crossing a triad, the envelope time series are divided into time windows of 10 min duration, with 5 min of overlap. This time window allows for a signal with a phase velocity of 260 m/s to cross a triad having a maximum arm length of 150 km. Time windows with low signal-to-noise (SNR) are discarded if the maximum amplitude for all three envelopes is less than a given cutoff value—a minimum allowable SNR of 2.0 is used here.

Cross-correlations are computed between each of three envelope pairs within the triad for time windows having adequate SNR, yielding the time delay between each sensor pair.

The signal envelopes are coherent if the time delays between station pairs satisfy the criterion

$$T_{ij} + T_{jk} + T_{ki} < t_{cons}, \tag{1}$$

(Cansi 1995) where the stations are denoted i, j, and k; T_{ij} is the delay time from station i to station j; and t_{cons} is a consistency cutoff. Ideally, the time delays sum to zero for a coherent signal but due to noise and signal variability between stations, the consistency requirement must be relaxed. A large consistency cutoff would lead to larger errors in the phase velocity and azimuth estimates. However, at a minimum, the consistency cutoff should be greater than the duration of the STA filter used to compute the envelopes, so the t_{cons} parameter was set to 25 s in this study. Signals detected using this criterion are assumed to be consistent with plane wave propagation across the triad, although nonplanar waves can also satisfy it. A standard tau-p array processing method (e.g., Havskov and Öttemoller 2010) is applied to the station time delays to compute the signal's phase velocity and heading across the triad, for each time window in which the time delays satisfy the consistency

criterion of Eq. 1. The azimuth and phase velocities are used to compute the equivalent beam-formed envelope for a point at the center of the triad, and the peak amplitude of the beam-formed envelope is identified as the arrival time.

This step is demonstrated in Fig. 21.3 for a triad located west of UTTR that registered both seismic and infrasound arrivals from the rocket motor blast. The triad configuration is shown to the left along with a line showing the direction to the known blast location. The 0.7–4 Hz band-passed waveforms for each of the numbered stations are shown in the upper right panel, with the corresponding envelopes. Three nonoverlapping time windows are shown. The small time delays in the first window suggest seismic signal; the larger time delays in the second suggest an infrasound signal. The final time window is discarded from further computation because the envelope maxima do not exceed the SNR cutoff. For the first two windows, the delay times between station pairs are estimated by cross-correlating the demeaned envelopes. Since the time delays satisfy the consistency criterion (Eq. 1), they are input to the tau-p method to find the phase velocity and bearing across the array for each window. These values are used to compute the beam-formed envelopes for a point at the centroid of the triad for each time window, as shown in the lower right panel. The peak amplitudes of each time window give the signal arrival times. As shown, the azimuths of the signals in the first two time windows agree with the ground truth value to within 5°. The phase velocity of the signal in the first time window is approximately 4 km/s, consistent

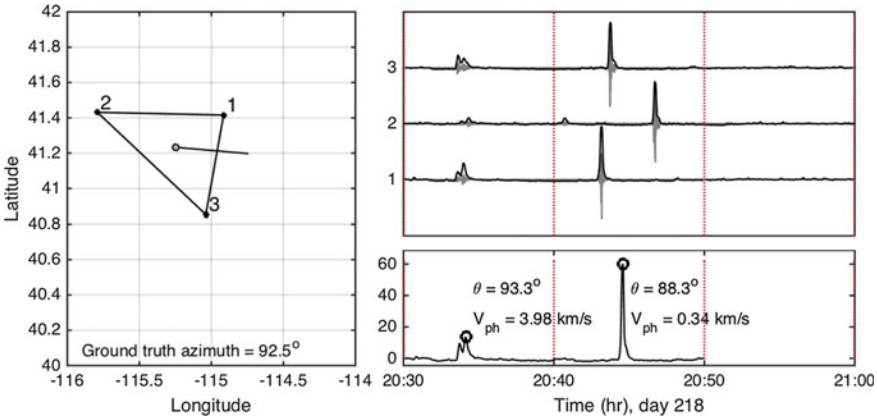

Fig. 21.3 Left: A triad configuration, with numbered stations. A gray circle marks the centroid location, with a line indicating the direction to UTTR. Top right: 0.7–4 Hz band-passed waveforms of the UTTR event and their envelopes. Dotted lines separate three nonoverlapping time windows. A seismic arrival is followed by an infrasound arrival at each station. Time delays were computed for each time window, and an azimuth and phase velocity was computed for each coherent signal. Bottom right: Beam-formed envelopes computed using the estimated azimuth and phase velocity for each time window, for a point corresponding to the center of the triad. Envelopes are computed only for time windows with a coherent arrival. A circle marking the maximum of the beam-formed envelope for each signal gives the estimate of the arrival time at the centroid location

with a shear wave, and the signal in the second time window has a phase velocity of 0.34 km/s, consistent with an infrasound arrival.

This method allows only for the detection of a single signal within a given time window. If both seismic and infrasound signals arrive within the same time window, the estimates of the phase velocity, azimuth, and arrival time will correspond to the one with the larger amplitude. For events that generate both seismic and infrasound energies, seismic signals are preferentially detected near the source where their amplitudes are higher, and infrasound signals are detected at greater ranges. Signals that propagate more slowly than infrasound signals can be eliminated by choosing a window duration that is too short for propagation across the entire triad. However, signals that travel faster than infrasound, like seismic signals, are not eliminated using the tau-p method. Other methods, such as an f-k analysis or correlation procedure (Brown et al. 2002; Gibbons et al. 2015), may be useful for separating multiple signal types that arrive in a single time window.

21.4.3 Assembling Signal Detections into Common Events

Each coherent detection at each triad has an associated phase velocity, azimuth, arrival time, an average cross-correlation computed from the three station pairs, an amplitude given by the peak amplitude of the beam-formed envelope, and a location, given by the centroid of the triad. From 6000 to 10000, unique coherent signals are detected daily over an average of 550 triads, with 287 10-min time windows analyzed at each triad. The use of seismic data to detect infrasound signals leads to the detection of far more coherent signals per day than for barometric data (de Groot-Hedlin and Hedlin 2015), because the data are contaminated with seismic signals.

Figure 21.4a shows all coherent signals with phase velocities from 300 m/s to 9000 m/s that occurred over a 1-h period from 20:30 to 21:30 UT on Julian day 218, 2007. That is, both seismic and infrasound signals are included. Figure 21.4b limits the coherent signal detections to those with phase velocities from 300 to 600 m/s, consistent with infrasound arrivals. Comparing Fig. 21.4a, b, the seismic signals can be distinguished from the infrasound arrivals by their very fast velocities across the array. A total of 883 coherent seismic and infrasound arrivals are shown in Fig. 21.4a, in comparison with only 324 signals consistent with infrasound propagation velocities in Fig. 21.4b; as indicated, many of the signals are seismic signals, which are not of interest to this study. The next step is to assemble the infrasound signal detections into groups, each consistent with a single source. Each group may include many infrasound propagation branches.

The detection of a coherent arrival at a single triad indicates either the passage of a signal across three stations or a chance correlation in a noisy dataset. To reduce the false alarm rate, AELUMA requires a lower threshold of N detections that are consistent with a single infrasound source to form a common event group. The choice of N is somewhat heuristic and depends on the source size of interest;

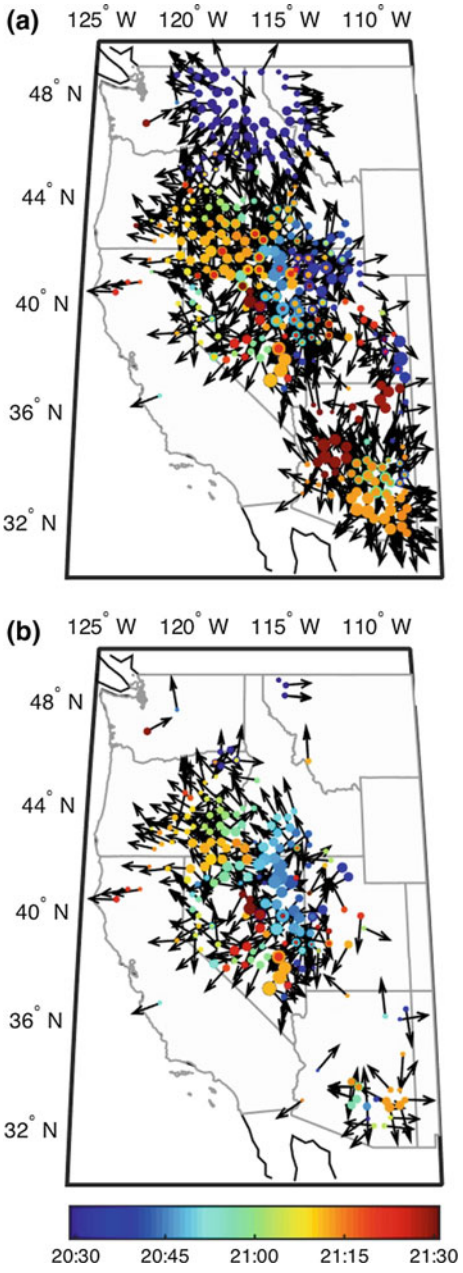

Fig. 21.4 Maps of signal detections in the 0.7–4 Hz band within the time period from 2030 to 2130 UT on day 218, 2007. Events on this day include a rocket motor fuel blast at UTTR at 20:33:03. Arrows show the direction of wave propagation across each triad. The circle size scales with SNR. The color scale shows the detection time on day 218. **a** All coherent signal detections with phase velocities ranging from 300 to 9000 m/s, which includes seismic and infrasound arrivals. **b** All coherent signal detections with phase velocities from 300 to 600 m/s, which eliminates seismic signals

N is set as low as 10 in this study, which limits events to those that were recorded across a region of at least 40,000 km^2. This choice leads to an event catalog that characterizes the acoustics of a region and also provides large infrasound events for further study.

Most signal detections on any given day are ultimately discarded as they are associated either with very small sources or noise. The task of finding sufficiently large infrasound sources for the catalog thus involves finding bundles of N or more detections consistent with a single source. The detection algorithm places a uniform grid of hypothetical source locations across the study area. For each test gridpoint, the distance and azimuth to the triad centroid is computed for all coherent signal detections, and a subset of detections with propagation azimuths consistent with travel from that gridpoint is found. An azimuth is consistent if it fits to within (A + *d*) degrees, where A is set to 10° in this study to accommodate errors in the azimuth estimates and deflections due to wind. The value *d* is the angle subtended by the distance between adjacent grid points, which increases with the coarseness of the search grid and decreases with the distance between the test gridpoint and the center of the triad.

The method of grouping detections into common events is illustrated in Fig. 21.5 for the infrasound detections shown in Fig. 21.4b, i.e., from 20:30 to 21:30 UT on Julian day 218, 2007, which includes signals from UTTR. The grid of test source locations is indicated by the red dots; the green circle indicates the known location of the UTTR blast. Figure 21.5a shows the subset of detections that are consistent with a source about one degree north and two degrees west of the known location; Fig. 21.5b shows those that are consistent with a grid point near the known location. There are no infrasound signal detections within about 100 km from the UTTR source, although faint infrasound signals may be seen in nearby recordings, see Fig. 21.2. Near the source, seismic amplitudes are larger than the infrasound arrivals, and the coherent signals have phase velocities that are consistent with seismic arrivals. As may be expected, far more detections are consistent with a source at the known location. If the subset had fewer than N members, the test point would be inconsistent with a source location and discarded from further computations for that day.

If there is a subset of at least N detections with azimuths that are consistent with the grid point being tested, the travel times are found for each member within the subset, for a set of potential source times t_k. The vector t_k is sampled at a uniform time sampling interval *dt*. The count $n(t_k)$ denotes the number of detections consistent with celerities between 250 and 340 m/s, for each time t_k. This range of celerities allows infrasound phases that travel along different paths through the atmosphere to be counted equally. This step is illustrated in Fig. 21.6. For each time t_k, AELUMA counts the number of detections within the subset between the minimum travel time as a function of range, given by $t_k - dt + R/340$ where R is the range in meters from the grid point to the triad centroids, and maximum travel time, given by $t_k + dt + R/250$. In Fig. 21.6, the maximum and minimum time

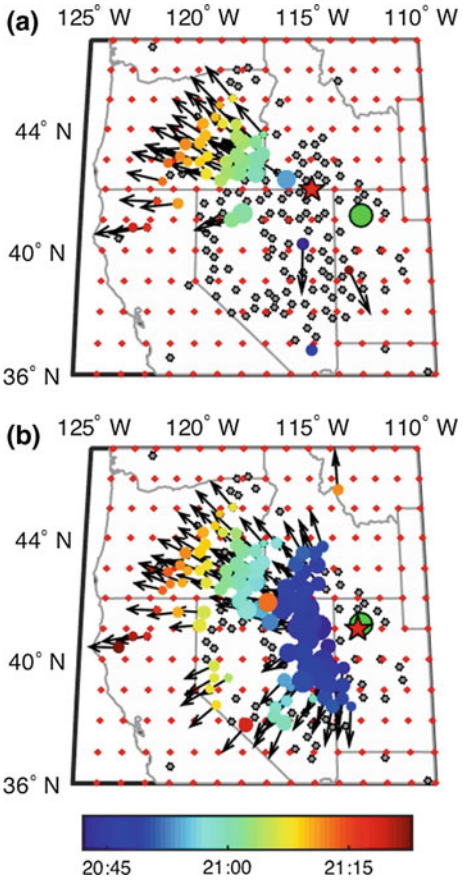

Fig. 21.5 Subsets of the detections shown in Fig. 21.4b, superimposed on a regular grid of test source points, shown by red dots, and the known UTTR source location, shown by green circles. Gray dots indicate the locations of all triad centroids with detections that have an azimuth that is inconsistent with the test gridpoint, marked by the red star. **a** The subset of detections with azimuths consistent with a source points at 42.0°N, −115°W. **b** The subset of detections with azimuths consistent with a source points at 41.0°N, −113°W, near the known source location

limits are shown for the times that yield the highest $n(t_k)$ value for each of the test locations shown in Fig. 21.5. If $n(t_k) < N$ for all potential source times, the grid point is discarded as inconsistent with an infrasound source location. The source time associated with the maximum $n(t_k)$ for the *ij*th grid point is the optimal source time for that gridpoint and is denoted T_{ij}. Figure 21.6b, for detections at a grid point near UTTR, shows that they do not fall along a straight line on a time versus distance plot, suggesting varying propagation paths.

The number of triads with detections that are consistent with an infrasound source at the *ij*th grid point for source time T_{ij} is denoted M_{ij} (T_{ij}). However, this value may be identical at several adjacent points so a penalty, equal to the rms azimuth misfit, is applied at each point to break ties between potential source locations. AELUMA defines a fitness level f_{ij} for each point with a group of at least N signal azimuths consistent with the *ij*th grid point, as

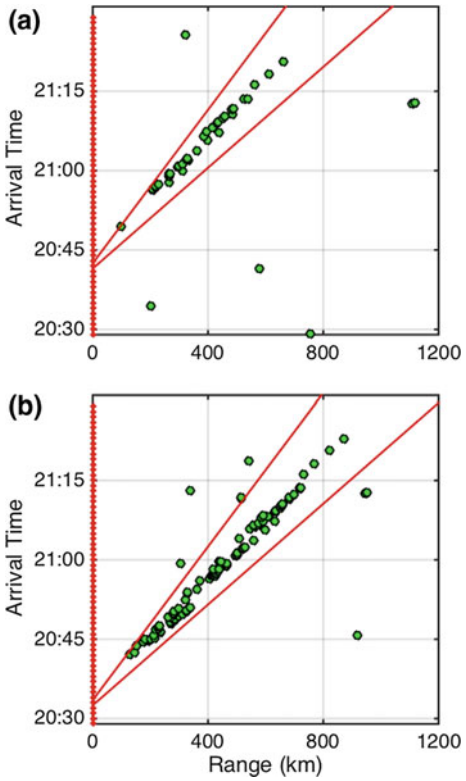

Fig. 21.6 Plots of arrival time versus range for detections with propagation azimuths corresponding to test grid points at **a** 42.0°N, −115°W, and **b** 41.0°N, −113°W, as shown in Fig. 21.5. The red dots at zero range indicate the vector of potential origin times t_k. The red lines bracket the minimum and maximum arrival times for the origin times that yield the highest number of detections within the bracket

$$f_{ij} = M_{ij}(T_{ij}) - \sqrt{\frac{\sum_{k=1}^{M} (\alpha_k - \alpha_{ij})^2}{M_{ij}(T_{ij})}} \tag{2}$$

where the second term is the rms azimuth misfit for triads within that group. The fitness level is zero if there are fewer than N detections with signal azimuths consistent with the point. Figure 21.7 shows a map of fitness levels computed for infrasound signals detected over a 4 h period from 20:00 to 24:00 UT on Julian day 218, 2007. The map suggests that there are at least two potential source locations: a larger one associated with the UTTR event and a smaller one to the south. There may, in fact, be more shots in this time span because events with small spatial separation but at different times overlap in this figure. The gridpoint with the highest fitness level is taken as an approximate source location and the value of T_{ij} at that point is taken as the initial estimate of the source time.

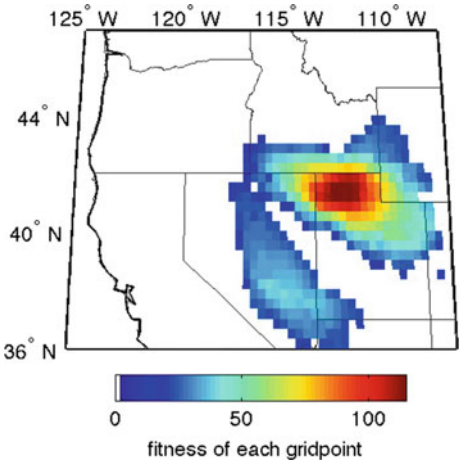

Fig. 21.7 A map of possible source locations for coherent signal detections found from 20:00 to 24:00 UT on Julian day 218, day 2007; this encompasses the 1 h of infrasound detections shown in Fig. 21.4b. The search area is discretized at three samples per degree in latitude and longitude. The fitness level is approximately the number of detections with propagation azimuths and arrival times that correspond to an infrasound source at each grid point. Areas where there are fewer than the minimum allowable detections to define an event group are shown in white

Figures 21.4 through 21.7 illustrate a single iteration of the event identification method. Each iteration identifies a single source time and location, along with its associated coherent detections. Following each iteration, the detections associated with the largest event group are removed from the ensemble and the remaining detections are used to locate another source. When no additional groups of at least N infrasound detections can be identified, the iterations are terminated.

The iterations are performed twice: once over spatially and temporally coarse grids to get rough estimates of the source parameters, and a second time to obtain more refined estimates. In this study, the coarse spatial grid is sampled at three grid points per degree in both latitude and longitude, with the limits of the grid covering the entire region covered by the TA, plus three degrees on each side. A time sampling interval of 60 s over an entire day is used to define the set of potential source times t_k. On the second pass, the grid is discretized into twenty points per degree, over a $3° \times 3°$ grid centered at the rough source location estimates found in the first pass, and a finer time sampling interval of 10 s over an 8 min time span centered at the coarse source time estimate. This has been amended from the initial AELUMA method (de Groot-Hedlin and Hedlin 2015), which sought to find fine-scale estimates of the source parameters by forcing uniform celerities. The revised method allows for a range of infrasound celerities, as in nature.

21.5 Results

21.5.1 Error Analysis Using UTTR Blasts

Events at UTTR are particularly useful for a study of AELUMA's accuracy because their locations are not only accurately recorded but their yields fall in a narrow range. Virtually, all blasts used in this study have explosive yields ranging from 17143 to 17688 kg. Acoustic signals from these large events are commonly recorded by seismometers to a range of 800 km or more (Hedlin and Drob 2014; Chunchuzov et al. 2014).

In this study period, there were 23 blasts at UTTR (12 in 2007 and 11 in 2008). All events occur through the summer season. Estimates of explosive yields for the first 21 blasts are listed in Table 21.1. Of these events, all but one had an explosive yield of over 17000 kg. The TA had moved too far to the east to reliably detect the final two blasts, mainly due to the fact that the summertime zonal winds carry the stratospherically ducted energy to the west of the source. Although some acoustic energy may be tropospherically ducted to the east due to the presence of the tropospheric jet stream, this wind generally decreases in magnitude and is less stable during the summer (Fee et al. 2013), so that TA detections more rare at stations to the east. By the time of the last two detonations, all TA stations located to the west of UTTR had been removed and moved east of the facility.

Table 21.1 also includes the AELUMA estimates of event origin time, misfit in time (in s), and misfit in location (in km). Origin times are typically late (16 of 21 detected events). The mean time misfit is 19 s with a standard deviation of 39 s. The time estimates have a positive bias because AELUMA picks the peak amplitude of the detected signal, not the signal onset, as discussed in de Groot-Hedlin and Hedlin (2015). As discussed by Hedlin and Drob (2014) and others, small-scale atmospheric structure disperses infrasonic signals, causing most of the wave packet to arrive later than the minimum travel time.

In contrast, the RTM method (Walker et al. 2011) located 10 of the 23 events (9 in 2007 and 1 in 2008). On average the RTM origin time estimates were 60 s early, which is within one time sample point, given that the data envelopes were decimated to 1 sample per 100 s. The mean AELUMA location, taken from the population of 21 events detected, was 8.6 km to the northwest of UTTR as shown in Fig. 21.8. This is only slightly greater than the average fine grid spacing of 5 km, and well under the mean TA station spacing (Fig. 21.8). The mean RTM location, taken from a population of 10 detected events, was 19.3 km to the east.

21.5.2 Event Detection in the Western United States

The TA was located in the western United States in 2007 and 2008, which is a very acoustically active part of the country (Walker et al. 2011). Just over 600 stations

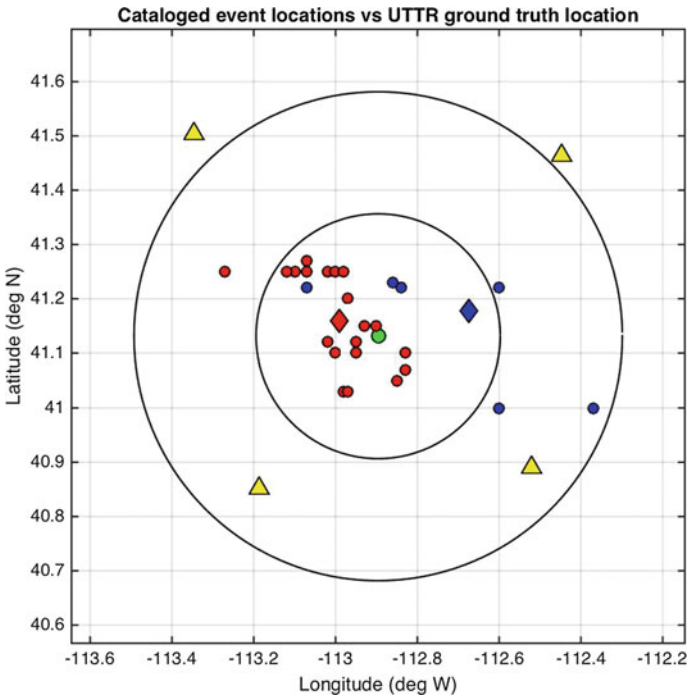

Fig. 21.8 Location estimates of the UTTR events that were detected by the AELUMA method (in red) and RTM (blue) plotted with the known location of the UTTR facility (green). The circles centered on UTTR mark range from the facility in 25 km increments. Mean estimated locations are represented by the diamond-shaped symbols. The four closest TA stations are shown as yellow triangles

operated for part or all of this time and 4966 triads were formed using these stations. An example event that was detected by 38 triads is shown in Fig. 21.9. This event was placed by AELUMA at 40.27°N, 113.02°W, which is about 100 km to the SSW of the UTTR facility. The cause of this event is unknown.

Figure 21.10 shows a histogram of acoustic sources detected by AELUMA in 2007 and 2008 in the western US. This map resembles the one in Walker et al. (2011) that shows significant activity in Nevada, Idaho, NW Utah, and southern California. The AELUMA catalog shows an additional site of activity near Socorro, New Mexico, which is the site of various explosive tests conducted by the Energetic Materials Research and Testing Center, EMRTC, located at 106.96°W 34.04°N, (personal communication, Jeff Johnson). Only sources consistent with detections at a minimum of 20 triads are plotted; smaller events are more poorly located, causing the hotspots to be blurred. Setting the lower threshold to 20 triads leads to 1686 events; at a threshold of 10 triads, 4791 events are found. In contrast, the RTM code found 901 events in this time period.

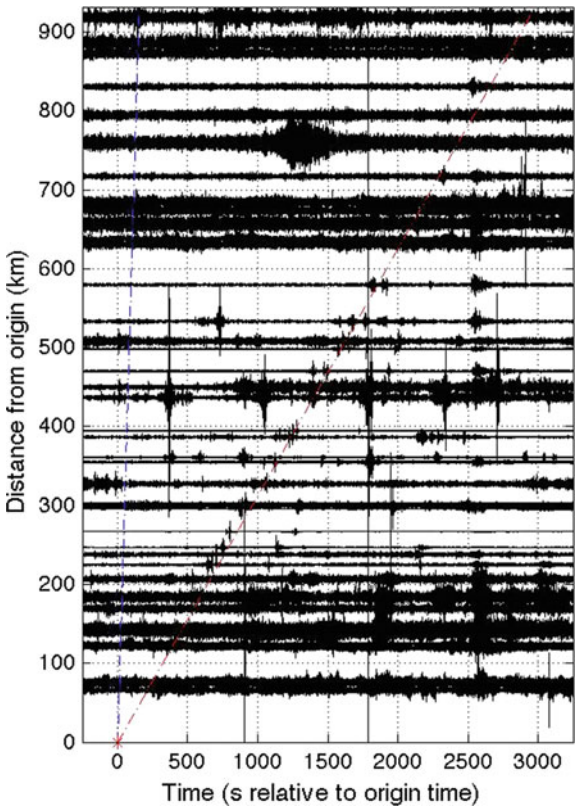

Fig. 21.9 Vertical component broadband seismic recordings of an unidentified event that occurred at 40.27°N, 113.02°W on JD 165, 2007 at 17:12:10 UT. The event was detected by 38 triads. The recordings have been bandpass filtered from 0.7 to 4 Hz and normalized to the same amplitude using data points lying within 250 s of the dashed red line which marks the average celerity of the detected signals

21.5.3 Acoustic Activity as a Function of Time

Seismic data for the entire 9-year time span from January 1, 2006 through December 31, 2014, were analyzed to examine acoustic activity across the entire continental United States. The TA moved eastward at an average rate of about 500 km/year during this time. The effect of this movement is shown in Fig. 21.11, which shows, in the upper panel, the longitude of the detected events as a function of time. In building the national catalog, all sources detected by at least 10 triads are considered. This lower limit is used because far fewer events, only 170, were detected in the east in 2012 through 2014 when the detection threshold was set to 20 triads. Using a threshold of N = 10 for the 9-year time span increased the number of detected events in this time span to 964, although it produces a blurred histogram as discussed in Sect. 21.5.2. In the lower panel of Fig. 21.11, a weekly count of detected events is shown, suggesting much higher acoustic activity in the western United States. The effect of seasonally varying stratospheric zonal winds is seen the lower panel, with increased numbers of detected events during the winter

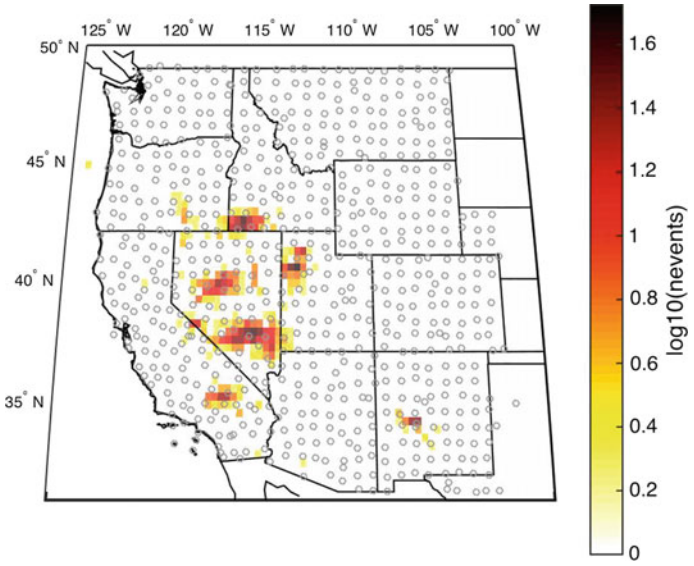

Fig. 21.10 Histogram of 1686 events detected in 2007 and 2008 by at least 20 triads. The catalog finds the same hotspots as detected by RTM and several more, such as the events located just west of Socorro, New Mexico. The histogram shows two sharp peaks in Utah, which are due to events at UTTR and the Dugway proving grounds (northern and southern peaks, respectively). There is considerably more activity in Nevada, with other concentrations of events in southern California, southern Idaho, and south-central Oregon. All stations in the TA that operated for at least of part of the 2 years are plotted

months, especially for the second through fifth years when the TA was fully deployed in the west. The rate at which events are detected surges when zonal winds place the bulk of the TA downwind of the most active source regions. There is relatively little activity detected by the seismometers from early 2011 through early 2013 as the network approached the Atlantic coast. In mid-2013 and 2014, the level of activity increased again in areas just off the Atlantic coast.

Figure 21.12 shows statistics on the time and day of detected events. The upper panel shows that most events occur after 08:00 local time, with the number of acoustic sources decreasing by the local mid-afternoon. The higher number of sources detected in daytime indicates that increased noise levels due to increased surface wind speeds during the day do not hamper the AELUMA algorithm. This is mainly due to the careful choice of frequency band chosen for our analysis; Fee and Garcés (2007) show that noise levels scale with wind speeds at frequencies below 0.3 Hz. The lower panel of Fig. 21.12 shows that the majority of events occurred from Monday through Friday.

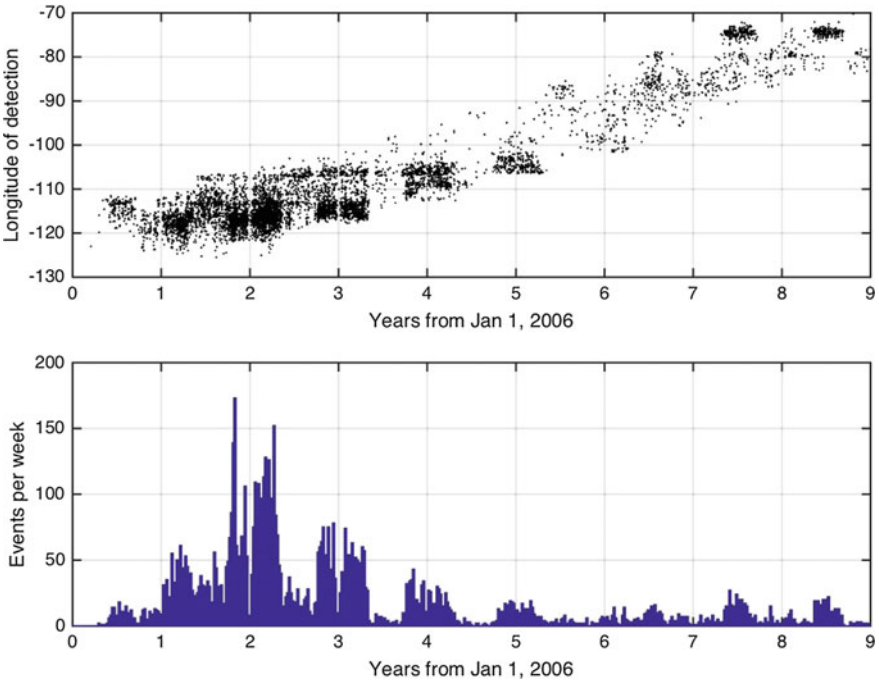

Fig. 21.11 The upper panel shows the longitude of events detected by the AELUMA method as a function of time from January 1, 2006 to December 31, 2014. The lower panel shows the number of events detected each week. The gradual shift to more eastern events is due to the movement of the TA. These results are for the 0.7–4.0 band and include events that were detected by at least 10 triads. In total, 7935 events were found. In comparison, 15430 events were found in the 2–8 Hz band and 1921 events in the 0.5–2.0 Hz band

21.5.4 US National Map of Acoustic Activity

Figure 21.13 shows a map of infrasonic activity across the continental United States for the 9-year time span beginning on January 1, 2006. During this time period, nearly 2,000 TA sites were occupied. This map, derived using a lower threshold of 10 triad detections, reveals new source regions not shown in Fig. 21.10. For example, source regions are observed in south-central New Mexico at the White Sands Missile Range. A concentration of activity in the Powder River Basin in eastern Wyoming due to coal mining is observed. Two areas of activity in Montana have not yet been identified. The hotspot, at 31.26°N, 103.25°W near Pecos, Texas is due to the use of explosives to make industrial diamonds (Paul Golden, SMU personal communication). The application of the AELUMA code to seismic data reveals far fewer acoustic hotspots in the east than were seen in de Groot-Hedlin and Hedlin (2015),

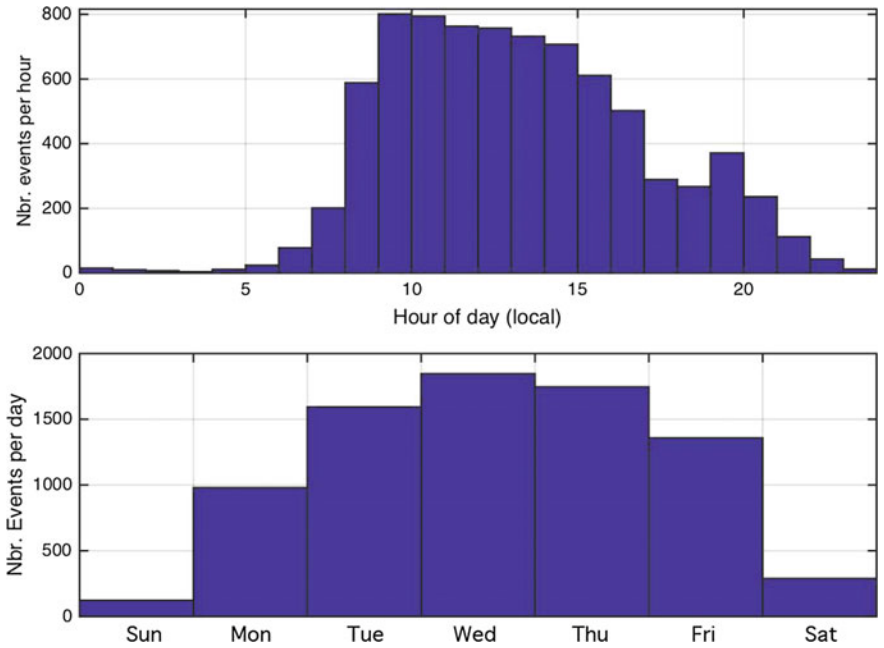

Fig. 21.12 Local time-of-day of detections by the AELUMA method occurrence rate as a function of time from January 1, 2006 to December 31, 2014 are shown in the upper panel. The lower panel shows the number of events detected each day of the week. These results are for event detections in the 0.7–4.0 Hz band and include sources that were detected by at least 10 triads. The distribution of events through the day and week is not uniform and points to anthropogenic activity

which used infrasonic data. The evidence of mining activity, and the intense acoustic activity in the Gulf of Mexico and off the Atlantic coast found in that study, is not seen here.

21.6 Discussion

21.6.1 The Detected Events

The time-of-day and day-of-week statistics clearly show that most infrasonic events that were detected in the western United States in 2007 and 2008 were anthropogenic, as also concluded by Walker et al. (2011). This includes the previously unreported source region located just west of Socorro, New Mexico. Further east, the level of activity detected using seismic data decreases significantly. Nationwide, most source regions are small and become active during normal working hours. Although the acoustic fingerprint of mankind was expected in the data, it is still

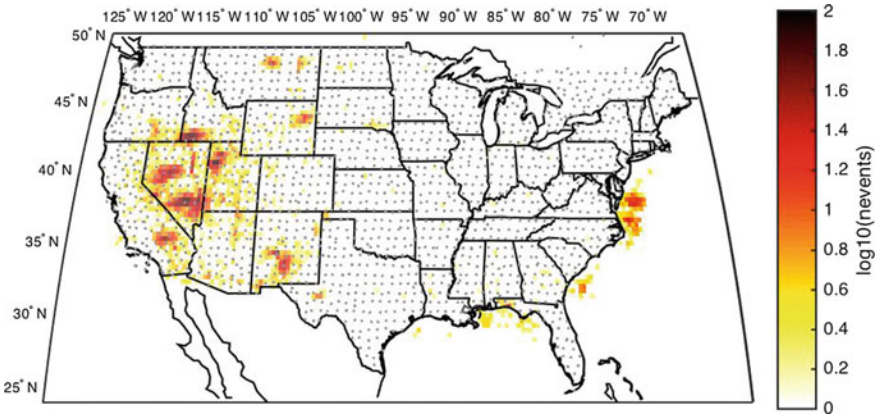

Fig. 21.13 A map of infrasound sources detected using seismic data during the 9-year period beginning on January 1, 2006, in the 0.7–4 Hz band. The lower threshold to define an event is 10 triads here, rather than 20 triads, as shown in Fig. 21.10. This allows smaller events to be seen, but blurs some of the acoustic hotspots observed in Fig. 21.10, because smaller events typically have poorer source location estimates. In total, 7935 events nationally were found in the 0.7–4 Hz band. Over 15000 events were found in the 2–8 Hz band; fewer than 2000 events were found in the 0.5–2 Hz band

surprising that sound waves from the largest of these events can be detected seismically at distances of several 100 to over 1000 km.

21.6.2 Sensitivity of AELUMA and RTM

A disadvantage of the RTM method, as applied by Walker et al. (2011), is that celerity is assumed to be constant across the TA. However, infrasound arrivals fall on distinct time branches (Hedlin et al. 2010) depending on their path through the atmosphere. Arrivals from different infrasonic branches at a given station may be separated by up to a 100 s. In order to ensure that all infrasound branches would stack coherently over ranges of hundreds of km, the RTM implementation of Walker et al. (2011) required that envelopes were severely smoothed, with one point per 100 s, which limited the detections to relatively larger source. By contrast, AELUMA requires only that the phase velocity is uniform over the aperture of any given triad. It allows for a range of celerities over hundreds of km of propagation without requiring that the envelopes be severely smoothed. Furthermore, AELUMA is fully automated and does not require the input of an analyst.

Comparing the number of events in the catalogs produced by AELUMA and RTM, and the relative number of UTTR events detected by the two methods, AELUMA is clearly more sensitive to weak signals from small events. Although the frequency band used in this analysis was slightly lower than the one used by

RTM (0.7–4 Hz vs. 1–5 Hz), it seems unlikely that this would significantly favor one approach over the other. The AELUMA code detected 21 of the 23 detonations that occurred at the UTTR facility in 2007 and 2008, including all 12 events in 2007 and the first 9 events in 2008. The last two events that year (on JD 254 and 261) were not detected because the TA was located mainly east of the UTTR, upwind of the summertime stratospheric winds, and tropospheric ducting was apparently insignificant. Also, the yield of those two final events is unknown. In comparison, the RTM approach (Walker et al. 2011) found only 10 of the events in total: 9 in 2007 (on JD 135, 155, 162, 177, 190, 197, 213, 225, and 239), and 1 in 2008 (on JD 168).

Of the entire population of 7935 events in the national AELUMA catalog in the 0.7–4 Hz band, at most 178 triads were used to define a single source location. More than half the events were detected by 10 to 20 triads. The lower limit of triads used to define a source location in this study is somewhat arbitrary. A threshold of 10 was chosen partly to reduce the computational load but also to reduce the false alarm rate. Location accuracy decreases as the number of triads used in the solution decreases.

21.6.3 Seismic Versus Infrasonic Data

In 2012 through 2014, the TA stations were equipped with both infrasonic and broadband seismic sensors. In a study of the acoustics of the eastern United States, de Groot-Hedlin and Hedlin (2015) used the infrasonic sensors to find considerable activity, both offshore and in mining regions. In this study, this analysis is repeated using vertical component seismic data. Although a careful comparison of the utility of using infrasonic versus seismic data for detecting atmospheric sources is beyond the scope of this paper, there is a significant difference in the size of the two catalogs. Using infrasonic data and a lower threshold of 20 triads to define a source location, 5666 events were found using AELUMA. Using the same parameters for seismic data, only 170 events were found. This large difference is attributable to poor acoustic-to-seismic coupling at the seismic stations in the eastern US. Given that infrasonic data were not available in the western US, it cannot be concluded that the coupling is poorer in the eastern US than the western US. Conversely, it cannot be concluded with certainty that the western US is significantly more acoustically active than the eastern US as it remains possible that the different activity levels (cf. Fig. 21.13) result from differences in acoustic-to-seismic coupling.

21.7 Conclusions

Although infrasonic signals near 1 Hz are uncorrelated between stations that are separated by more than several km, this study confirms that signal envelopes are correlated to distances of at least 70 km. This fact is exploited to develop a new approach to signal detection and event location that, in broad terms, finds and characterizes coherent signals recorded by small three-element arrays within a sensor network, then combines information from many similar arrays distributed across the network to estimate the source time and location corresponding to these coherent detections. The efficacy of migration methods, such as RTM, to detect and locate sources is well known. However, considering the relative performance of AELUMA and RTM (specifically, the number of events detected during 2007 and 2008 and the accuracy of the source estimates), it appears that this use of local wave-field characteristics gives AELUMA a critical advantage.

Our national catalog of infrasonic activity confirms the general features of the western US catalog first identified by Walker et al. (2011). Infrasonic activity is not uniformly distributed but is concentrated in "hotspots". Concentrations of infrasonic sources are detected across the country but are largest in the west. The concentration of sources during the mid-day each week from Monday through Friday indicates that most activity is anthropogenic. Aside from these diurnal and weekly cycles, the seasonal effect of reversing zonal winds is clearly observed. For this reason, we expect that the catalog should provide a wealth of data for tests of atmospheric models as well as studies of the sources themselves.

The source parameters listed in the catalogs developed here and in de Groot-Hedlin and Hedlin (2015) are more accurate for acoustic events that lie within the network, surrounded by stations, than for those on the edge of the network or in the far field. They do not have the precision of ground truth information, as in Gibbons et al. (2019). There is a place for catalogs produced by any method, such as RTM and AELUMA, in nuclear monitoring. As discussed by Walker et al. (2011), an area of ongoing interest in the infrasound community is distinguishing events that are possibly nuclear in origin from the clutter of other anthropogenic and natural events. These catalogs clearly define acoustic hotspots that would likely clutter data recorded by the region's IMS infrasound arrays. Event catalogs have historically been important in geophysical research by providing a starting point for many studies—e.g., studies of fine-scale atmospheric structure using dispersed infrasound signals and fine-scale structure due to gravity waves (e.g., Drob et al. 2013; Hedlin and Walker 2013), and studies of variations of large-scale atmospheric structure using infrasonic wave trains.

Acknowledgements This material is based upon work supported by the National Science Foundation under Grant No. EAR-1358520. We thank Relu Burlacu for providing ground truth information on the explosions at UTTR. This study would not have been possible without the high-quality data from the USArray TA. The TA is part of the Incorporated Research Institutions for Seismology (IRIS) EarthScope program. The authors thank Jelle Assink for a constructive review.

Supporting Information

National event catalogs in three bands (0.5–2.0 Hz, 0.7–4.0 Hz, and 2–8 Hz) computed using seismic data collected from 2006 through 2014. Catalog of events in the eastern United States computed using infrasonic data collected in 2012, 2013, and 2014. The AELUMA code is now available on request through product@iris.washington.edu.

Appendix

The AELUMA method is applicable to a wide range of network configurations and signal types, given that parameters are set correctly for signal type sought and the array configuration. Table 21.2 describes the main parameters needed; values used for this study are listed in the final column. The AELUMA code is available on request through product@iris.washington.edu.

Table 21.2 AELUMA parameters

Parameter	Description	Suggested range	Value
			(this study)
R	Mean interstation distance	Network dependent	70 km
f_{min}–f_{max}	Signal frequency band	Signal dependent	0.7–4 Hz
v_{min}	Minimum phase velocity	Signal dependent	0.25 km/s
v_{max}	Maximum phase velocity	Signal dependent	0.8 km/s
c_{min}	Minimum celerity	Signal dependent	0.25 km/s
c_{max}	Maximum celerity	Signal dependent	0.34 km/s
R_{max}	Maximum triad arm length	(2–3) × R	150 km
t_{STA}	Short-term average smoothing	(2–8)/f_{min}	10 s
t_{LTA}	Long-term average smoothing	(40–80) × t_{STA}	600 s
t_{win}	Time window	max(R_{max}/v_{min}, 15 * t_{STA})	600 s
t_{step}	Time step between windows	$t_{win}/2$	300 s
t_{cons}	Consistency limit (see Eq. 1)	$t_{win}/10 > t_{cons} > t_{STA}$	25 s
φ_{min}	Minimum interior angle for triad	10–20°	15°
φ_{max}	Maximum interior angle for triad	130–150°	130°
N	Minimum #triads to identify a source	10–25	10 and 20
A	Azimuth misfit threshold (see Fig. 21.5)	10–15°	10°
G_{course}	Course spatial grid	R/4–R/2	0.33°
G_{fine}	Fine spatial grid	$G_{course}/10$–$G_{course}/5$	0.05°

The phase and celerity values depend on the signal type sought. For example, for infrasound, the true phase velocities range from about 320 m/s and up, depending on whether the signal propagates horizontally across the triad or has steep incidence from above. The phase velocities are allowed a wide range, to allow for errors in phase velocity and propagation angle across the triad that derives from the imperfect fit to Eq. 1.

References

Arrowsmith SJ, Whitaker R, Taylor SR, Burlacu R, Stump B, Hedlin M, Randall G, Hayward C, ReVelle D (2008) Regional monitoring of infrasound events using multiple arrays: application to Utah and Washington State. Geophys J Int 175:291–300. https://doi.org/10.1111/j.1365-246X.2008.03912.x

Arrowsmith SJ, Johnson JB, Drob DP, Hedlin MAH (2010) The seismoacoustic wavefield: a new paradigm in studying geophysical phenomena. Rev Geophys. 48:RG4003. https://doi.org/10.1029/2010rg000335

Arrowsmith S, Euler G, Marcillo O, Blom P, Whitaker R, Randall G (2015) Development of a robust and automated infrasound event catalogue using the International Monitoring System. Geophys J Int 200:1411–1422. https://doi.org/10.1093/gji/ggu486

Assink J, Smets P, Marcillo O, Weemstra C, Lalande J-M, Waxler R, Evers LG (2019) Advances in infrasonic remote sensing methods. In: Le Pichon A, Blanc E, Hauchecorne A (eds) Infrasound monitoring for atmospheric studies, 2nd edn. Springer, Dordrecht, pp 605–632

Assink JD, Waxler R, Frazier WG, Lonzaga J (2013) The estimation of upper atmospheric wind model updates from infrasound data. J Geophys Res Atmos 118:10707–10724. https://doi.org/10.1002/jgrd.50833

Brown DJ, Katz CN, Le Bras R, Flanagan MP, Wang J, Gault AK (2002) Infrasonic signal detection and source location at the Prototype International Data Centre. Pure Appl Geophys. 159:1081–1125. https://doi.org/10.1007/s00024-002-8674-2

Busby RW, Vernon FL, Newman RL, Astiz L (2006) Earth-Scope's USArray: advancing eastward. EOS, Trans Am Geophys Un 87(52), Fall Meeting, Supplement, Abstract U41B-0820

Cansi Y (1995) An automatic seismic event processing for detection and location: the P.M.C.C. method. Geophys Res Lett 22:1021–1024

Campus P, Christie DR (2010) In: Le Pichon A, Blanc E, Hauchecorne A (eds) Worldwide observations of infrasonic waves. Springer, pp 185–234. https://doi.org/10.1007/978-1-4020-9508-5_6

Ceranna L, Le Pichon A, Green DN, Mialle P (2009) The Buncefield explosion: a benchmark for infrasound analysis across central Europe. Geophys J Int 177(2):491–508. https://doi.org/10.1111/j.1365-246X.2008.03998.x

Christie DR, Campus P (2010) The IMS infrasound network: design and establishment of infrasound stations. In: Le Pichon A, Blanc E, Hauchecorne A (eds) Infrasound monitoring for atmospheric studies. Springer, pp 27–72. https://doi.org/10.1007/978-1-4020-9508-5_2

Chunchuzov I, Kulichkov S (2019) Internal gravity wave perturbations and their impacts on infrasound propagation in the atmosphere. In: Le Pichon A, Blanc E, Hauchecorne A (eds) Infrasound monitoring for atmospheric studies, 2nd edn. Springer, Dordrecht, pp 551–590

Chunchuzov I, Kulichkov S, Popov O, Hedlin M (2014) Modeling propagation of infrasound signals observed by a dense seismic network. J Acoust Soc Am 135(1)

Chunchuzov I, Kulichkov S, Perepelkin V, Popov O, Firstov P, Assink JD, Marchetti E (2015) Study of the wind velocity-layered structure in the stratosphere, mesosphere, and lower thermosphere by using infrasound probing of the atmosphere. J Geophys Res Atmos 120:8828–8840. https://doi.org/10.1002/2015JD023276

Crampin S (1966) Higher-mode seismic surface waves from atmospheric nuclear explosions over Novaya Zemlya. J Geophys Res 71:2951–2958

Cochran ES, Shearer PM (2006) Infrasound events detected with the Southern California Seismic Network. Geophys Res Lett 33:L19803. https://doi.org/10.1029/2006GL026951

de Groot-Hedlin CD, Hedlin MAH, Walker KT, Drob DD, Zumberge MA (2008) Evaluation of infrasound signals from the shuttle Atlantis using a large seismic network. J Acoust Soc Am 124:1442–1451. https://doi.org/10.1121/1.2956475

de Groot-Hedlin CD, Hedlin MAH, Drob D (2010) Atmospheric variability and infrasound monitoring. In: Le Pichon A, Blanc E, Hauchecorne A (eds) Infrasound monitoring for atmospheric studies. Springer, New York, pp 475–507. https://doi.org/10.1007/978-1-4020-9508-5_15

de Groot-Hedlin CD, Hedlin MAH, Walker KT (2013) Detection of gravity waves across the USArray: a case study. Earth Planet Sci Lett. http://dx.doi.org/10.1016/j.epsl.2013.06.042

de Groot-Hedlin CD, Hedlin MAH (2014a) Infrasound detection of the Chelyabinsk meteor at the USArray. Earth Planet Sci Lett 402:337–345

de Groot-Hedlin CD, Hedlin MAH (2014b) Detection of seismic and infrasound sources at the USArray Transportable Array, 2016 AGU meeting

de Groot-Hedlin CD, Hedlin MAH (2015) A method for detecting and locating geophysical events using groups of arrays. Geophys J Int 203:960–971. https://doi.org/10.1093/gji/ggv345

Delclos C, Blanc E, Broche P, Glangeaud F, Lacoume JL (1990) Processing and interpretation of microbarograph signals generated by the explosion of Mount St. Helens. J Geophys Res 95 (D5):5485–5494. https://doi.org/10.1029/JD095iD05p05485

Donn WL, Rind D (1971) Natural infrasound as an atmospheric probe. Geophys J R Astron Soc 26:111–133

Drob DP, Picone JM, Garcés M (2003) Global morphology of infrasound propagation. J Geophys Res Atmos 108(D21):4680. https://doi.org/10.1029/2002JD003307

Drob DP, Broutman D, Hedlin MAH, Winslow NW, Gibson RG (2013) A method for specifying atmospheric gravity-wave fields for long-range infrasound propagation calculations. J Geophys Res. https://doi.org/10.1029/2012JD018077

Drob DP, Meier RR, Picone JM, Garcés MM (2010) Inversion of infrasound signals for passive remote sensing. In: Le Pichon A, Blanc E, Hauchecorne A (eds) Infrasound monitoring for atmospheric studies. Springer, New York, pp 701–731. https://doi.org/10.1007/978-1-4020-9508-5_24

Edwards WN, Eaton DW, McCausland PJ, ReVelle DO, Brown PG (2007) Calibrating infrasonic to seismic coupling using the Stardust sample return capsule shockwave: implications for seismic observations of meteors. J Geophys Res 112(B10306):1–13. https://doi.org/10.1029/2006JB004621

Edwards WN, de Groot-Hedlin CD, Hedlin MAH (2014) Forensic investigation of a probable meteor sighting using USArray acoustic data. Seismol Res Lett 85:1012–1018

Evers LG, Haak HW (2005) The detectability of infrasound in The Netherlands from the Italian volcano Mt. Etna. J Atmos Solar-Terr Phys 67:259–268

Evers LG, Haak HW (2010) The characteristics of infrasound, its propagation and some early history. In: Le Pichon A, Blanc E, Hauchecorne A (eds) Infrasound monitoring for atmospheric studies. Springer, New York, pp 3–27. https://doi.org/10.1007/978-1-4020-9508-5_1

Fee D, Garcés M (2007) Infrasonic tremor in the diffraction zone. Geophys Res Lett 34:L16826. https://doi.org/10.1029/2007GL030616

Fee D, Matoza RS (2013) An overview of volcano infrasound; from Hawaiian to Plinian, local to global. J. Volcanol Geotherm Res 249:123–139. https://doi.org/10.1016/j.jvolgeores.2912.09.002

Fee D, Waxler R, Assink J, Gitterman Y, Given J, Coyne J, Mialle P, Garcés M, Drob D, Kleinert D, Hofstetter R, Granard P (2013) Overview of the 2009 and 2011 Sayarim infrasound calibration experiments. J Geophys Res Atmos 118:6122–6143. https://doi.org/10.1002/jgrd.50398

Fee D, Haney M, Matoza R, Curt Szuberla C, Lyons J, Waythomas C (2016) Seismic envelope-based detection and location of ground-coupled airwaves from Volcanoes in Alaska. Bull Seismol Soc Am. https://doi.org/10.1785/0120150244

Fricke JT, Evers LG, Wapenaar K, Simons DG (2014) Infrasonic interferometry applied to microbaroms observed at the Large Aperture Infrasound Array in the Netherlands. J Geophys Res Atmos 119:9654–9665. https://doi.org/10.1002/2014JD021663

Garcés M, Willis M, Hetzer C, Le Pichon A, Drob D (2004) On using ocean swells for continuous infrasonic measurements of winds and temperature in the lower, middle, and upper atmosphere. Geophys Res Lett 31:L19304. https://doi.org/10.1029/2004GL020696

Green D, Vergoz J, Gibson R, Pichon AL, Ceranna L (2011) Infrasound radiated by the Gerdec and Chelopechene explosions: propagation along unexpected paths. Geophys J Int 185:890–910. https://doi.org/10.1111/j.1365-246X.2011.04975.x

Gibbons SJ, Kværna T, Mykkeltveit S (2015) Could the IMS infrasound stations support a global network of small aperture seismic arrays. Seismol Res Lett 86. https://doi.org/10.1758/0220150068

Gibbons S, Kværna T, Näsholm P (2019) Characterization of the infrasonic wavefield from repeating seismo-acoustic events. In: Le Pichon A, Blanc E, Hauchecorne A (eds) Infrasound monitoring for atmospheric studies, 2nd edn. Springer, Dordrecht, pp 387-407

Hagerty MT, Kim WY, Martysevich P (2002) Infrasound detection of large mining blasts in Kazakstan. Pure Appl Geophys 159(5):1063–1079. https://doi.org/10.1007/s00024-002-8673-3

Havskov J, Öttemoller L (2010) Routine data processing in earthquake seismology. Springer. https://doi.org/10.1007/978-90-481-8697-6_1

Hedlin MAH, Walker K (2013) A study of infrasonic anisotropy and multipathing in the atmosphere using seismic networks. Philos Trans R Soc A 371:20110542. https://doi.org/10.1098/rsta.2011.0542

Hedlin MAH, Drob D, Walker K, de Groot-Hedlin C (2010) A study of acoustic propagation from a large bolide in the atmosphere with a dense seismic network. J Geophys Res 115:B11312. https://doi.org/10.1029/2010JB007669

Hedlin MAH, Drob D (2014) Statistical characterization of atmospheric gravity waves by seismoacoustic observations. J Geophys Res Atmos 119. https://doi.org/10.1002/2013jd021304

Ishihara Y, Furumoto M, Sakai S, Tsukada S (2004) The 2003 Kanto large bolide's trajectory determined from shockwaves recorded by a seismic network and images taken by a video camera. Geophys Res Lett 31:L14702, 0094-8276

Kulichkov SN, Chunchuzov IP, Pupov OI (2010) Simulating the influence of an atmospheric fine inhomogeneous structure on long-range propagation of pulsed acoustic signals. Izv Atmos Ocean Phys 46:60–68. https://doi.org/10.1134/S0001433810010093

Lalande J-M, Waxler R (2016) The interaction between infrasonic waves and gravity wave perturbations: application to observations using UTTR rocket motor fuel elimination events. J Geophys Res Atmos 121:5585–5600. https://doi.org/10.1002/2015JD024527

Lee DT, Schachter BJ (1980) Two algorithms for constructing a Delaunay triangulation. Int J Comput Inf Sci 9:219–242

Le Pichon A, Garcés M, Blanc E, Barthelemy M, Drob DP (2002) Acoustic propagation and atmosphere characteristics derived from infrasonic waves generated by the Concorde. J Acoust Soc Am 111:629–641

Le Pichon A, Blanc E, Drob D (2005a) Probing high-altitude winds using infrasound. J Geophys Res 110. https://doi.org/10.1029/2005JD006020

Le Pichon A, Blanc E, Drob D, Lambotte S, Dessa JX, Lardy M, Bani P, Vergniolle S (2005b) Infrasound monitoring of volcanoes to probe high-altitude winds. J Geophys Res 110. https://doi.org/10.1029/2004JD005587

Le Pichon A, Herry P, Mialle P, Vergoz J, Brachet N, Garcés M, Drob D, Ceranna L (2005c) Infrasound associated with 2004–2005 large Sumatra earthquakes and tsunami. Geophys Res Lett 32:L19802. https://doi.org/10.1029/2005GL023893

Le Pichon A, Vergoz J, Blanc E, Guilbert J, Ceranna L, Evers L, Brachet N (2009) Assessing the performance of the International Monitoring System's infrasound network: geographical coverage and temporal variabilities. J Geophys Res 114:D08112. https://doi.org/10.1029/2008JD010907

Marchetti E, Ripepe M, Campus P, Le Pichon A, Brachet N, Blanc E, Gaillard P, Mialle P, Husson P (2019) Infrasound monitoring of volcanic eruptions and contribution of ARISE to the volcanic ash advisory centers. In: Le Pichon A, Blanc E, Hauchecorne A (eds) Infrasound monitoring for atmospheric studies, 2nd edn. Springer, Dordrecht, pp 1141–1162

Marty J (2019) The IMS infrasound network: current status and technological developments. In: Le Pichon A, Blanc E, Hauchecorne A (eds) Infrasound monitoring for atmospheric studies, 2nd edn. Springer, Dordrecht, pp 3–62

Matoza RS, Garcés MA, Chouet BA, D'Auria L, Hedlin MAH, de Groot-Hedlin C, Waite GP (2009) The source of infrasound associated with long-period events at Mount St. Helens. J Geophys Res 114:B04305. https://doi.org/10.1029/2008JB006128

Matoza R, Green D, Le Pichon A, Shearer PM, Fee D, Mialle P, Ceranna L (2017) Automated detection and cataloging of global explosive volcanism using the International Monitoring System infrasound network. J Geophys Res 122:2946–2971. https://doi.org/10.1002/2016JB013356

Matoza R, Fee D, Green D, Mialle P (2019) Volcano infrasound and the international monitoring system. In: Le Pichon A, Blanc E, Hauchecorne A (eds) Infrasound monitoring for atmospheric studies, 2nd edn. Springer, Dordrecht, pp 1023–1077

Millet C, Robinet J-C, Roblin C (2007) On using computational aeroacoustics for long-range propagation of infrasounds in realistic atmospheres. Geophys Res Lett 34:L14814. https://doi.org/10.1029/2007GL029449

Öttemoller L, Evers LG (2008) Seismo-acoustic analysis of the Buncefield oil depot explosion in the UK, 2005 December 11. Geophys J Int 172:1123–1134

Park J, Arrowsmith SJ, Hayward C, Stump BW, Blom P (2014) Automatic infrasound detection and location of sources in the western United States. J Geophys Res Atmos 119:7773–7798. https://doi.org/10.1002/2013JD021084

Park J, Stump BW (2015) Seasonal variations of infrasound detections and their characteristics in the western US. Geosci J 19:97. https://doi.org/10.1007/s12303-014-0034-6

Pasko VP (2012) Infrasonic waves generated by supersonic auroral arcs. Geophys Res Lett 39:L19105. https://doi.org/10.1029/2012GL053587

Pilger C, Ceranna L, Ross JO, Le Pichon A, Mialle P, Garcés MA (2015) CTBT infrasound network performance to detect the 2013 Russian fireball event. Geophys Res Lett 42:2523–2531. https://doi.org/10.1002/2015GL063482

Pilger C, Ceranna L, Le Pichon A, Brown P (2019) Large meteoroids as global infrasound reference events. In: Le Pichon A, Blanc E, Hauchecorne A (eds) Infrasound monitoring for atmospheric studies, 2nd edn. Springer, Dordrecht, pp 451–470

Revelle DO, Brown PG, Spurny P (2004) Entry dynamics and acoustics/infrasonic/seismic analysis for the Neuschwanstein meteorite fall. Meteorit Planet Sci 39:1605–1626

Silber E, Brown P (2019) Infrasound monitoring as a tool to characterize impacting near-earth objects (NEOs). In: Le Pichon A, Blanc E, Hauchecorne A (eds) Infrasound monitoring for atmospheric studies. 2nd edn. Springer, Dordrecht, pp 939–986

Smets PSM, Assink JD, Le Pichon A, Evers LG (2016) ECMWF SSW forecast evaluation using infrasound. J Geophys Res Atmos 121:4637–4650. https://doi.org/10.1002/2015jd024251

Sutherland LC, Bass HE (2004) Atmospheric absorption in the atmosphere up to 160 km. J Acoust Soc Am 115:1012–1032

Vergoz J, Le Pichon A, Millet C (2019) The antares explosion observed by the USArray: an unprecedented collection of infrasound phases recorded from the same event. In: Le Pichon A,

Blanc E, Hauchecorne A (eds) Infrasound monitoring for atmospheric studies, 2nd edn. Springer, Dordrecht, pp 349–386

Vernon F, Tytell J, Busby B, Eakins J, Hedlin M, Muschinski A, Walker K, Woodward B (2012) Scientific viability of the USArray Transportable Array Network as a real-time weather monitoring platform. In: 92nd American meteorological society annual meeting, American Meteor Society, New Orleans, La. https://ams.confex.com/ams/92Annual/webprogram/Paper200044.html

Walker K, Hedlin MAH, de Groot-Hedlin CD, Vergoz J, Le Pichon A, Drob D (2010) Source location of the 19 February 2008 Oregon bolide using seismic networks and infrasound arrays. J Geophys Res. https://doi.org/10.1029/2010jb007863

Walker KT, Shelby R, Hedlin M, de Groot-Hedlin C, Vernon F (2011) Western U.S. infrasonic catalog: illuminating infrasonic hot spots in the western U.S. with the USArray. J Geophys Res 116:B12305. https://doi.org/10.1029/2011JB008579

Walker KT, Le Pichon A, Kim TS, de Groot-Hedlin C, Che Il-Y, Garcés M (2013) An analysis of ground shaking and transmission loss from infrasound generated by the 2011 Tohoku earthquake. J Geophys Res Atmos 118:12805–12815. https://doi.org/10.1002/2013JD020187